Perturbed-angular-distribution measurements of the chemical shift of iron in the disulfides FeS_2 (pyrite) and RuS_2 (laurite)

W. Müller, H. H. Bertschat, K. Biedermann, R. Kowallik, E. Lahmer-Naim, H.-E. Mahnke, S. Seeger, and W.-D. Zeitz
Bereich Schwerionenphysik, Abteilung Festkörperphysik mit Schweren Ionen, Hahn-Meitner-Institut Berlin, Glienicker Strasse 100, D-1000 Berlin, Federal Republic of Germany

S. Fiechter and H. Tributsch
Bereich Photochemische Energieumwandlung, Abteilungen Solare Energetik and Materialforschung, Hahn-Meitner-Institut Berlin, Glienicker Strasse 100, D-1000 Berlin 39, Federal Republic of Germany
(Received 7 November 1989)

Measurements of the temperature dependence of the chemical shift at Fe nuclei in FeS_2 (pyrite) and Fe impurities in RuS_2 (laurite) were performed on high-purity synthetic single-crystal samples using the perturbed-angular-distribution method. Equivalent, considerably negative, and temperature-independent chemical shifts were observed in both hosts, which we attribute to strong van Vleck paramagnetism. Bulk susceptibility data at low temperatures show no local moment formation at Fe sites due to nonstoichiometric sulfur content. The results are evaluated with respect to the photoactive properties of these materials and the requirements for solar-energy applications.

I. INTRODUCTION

The iron sulfides form a class of chemical compounds that show a large variety of very interesting magnetic properties depending sensitively on the sulfur content. The iron monosulfides (FeS_{1-x}) have antiferromagnetic and ferrimagnetic ordered phases with complex magnetic and structural phase transitions.[1,2] The iron disulfide, pyrite (FeS_2), and the ruthenium disulfide, laurite (RuS_2), essentially are nonmagnetic semiconductors.[3-5] Both compounds have attracted much interest in recent years as promising candidates for future photovoltaic or photocatalytic materials.[6,7] Their high absorption coefficient, which exceeds 10^5 cm^{-1} at energies $h\nu > 1$ eV, could especially enable the application of these sulfides as absorber materials in thin layer photovoltaic devices. However, the properties of these compounds are strongly affected by the exact stoichiometry of their constituents, by impurity contamination, and by the preparation technique.[7] Extensive experimental work has been preformed and many calculations within highly developed electronic structure models have been performed to understand the intrinsic properties of these materials.[8-10] Experimental results on solid-state, chemical, photoelectric, and photochemical properties of FeS_2 and RuS_2 (see Table I) do not reveal largely equivalent electronic properties of these semiconducting materials. As compared to the rare and expensive RuS_2, the disadvantage of the abundant FeS_2 is its sulfur deficiency and the high dark current. As a consequence, low photovoltage is generated in liquid and solid-state devices and it is difficult to produce p-type material. The reason for the small photovoltage has tentatively been explained in terms of an interfering band within the forbidden region. Since so far FeS_2 was believed to be contaminated with FeS, there was reason to assume that FeS is responsible for the impurity band. (The existence of RuS is unknown.) Another explanation was the hypothesis that pyrite does not really have a low-spin configuration: A certain amount of unpaired spins, eventually caused by a deviation from the ideal composition, introduces a band in the forbidden region which diminishes the theoretically expected photovoltage.

Hyperfine interaction methods may contribute to the understanding of the materials under consideration, because they *locally* probe the electronic properties of the constituents of the compound. The determination of hyperfine fields may serve as a very sensitive test for electronic structure calculations.[8]

Mössbauer experiments have demonstrated that pyrite is nonmagnetic. The electric-field gradient, which is due to a trigonal distortion of the octahedral sulfur complex, was measured.[3,4,11] In agreement with these results it is generally believed that the Fe ion is forced to be in the divalent low-spin configuration by the repulsion of electrons from the d_{z^2} and the $d_{x^2-y^2}$ iron levels through sulfur ions. Accordingly, band-structure and molecular-orbital calculations show a completely filled t_{2g} band on top of the valence band of pure $3d$ electron character. The antibonding e_g–S σ hybrid forms the bottom of the conduction band due to the large crystal-field splitting.[8-10] Similar arguments apply to laurite. Thus both compounds have to be considered as nonmagnetic semiconductors with a band gap of 0.95 eV (Ref. 12) and 1.3 eV,[7] respectively.

In an externally applied magnetic field H_{ext}, magnetic shielding effects such as diamagnetic shielding and van Vleck paramagnetism occur.[13] Therefore at the iron site the chemical shift σ leads to an effective magnetic field $H_{eff} = H_{ext}(1-\sigma)$. In a Mössbauer experiment with ^{57}Fe,

TABLE I. Comparison of properties of FeS_2 and RuS_2.

Properties	FeS_2	RuS_2
Band gap	0.95 eV	1.3 eV
Quantum efficiency	90%	10–20%
Photocurrent density (air mass 0)	40 mA cm^{-2}	3.3 mA cm^{-2}
Dark currents in Schottky barriers	High currents	Low currents
H treatment	Improvement of interface liquid/solid in electrochemical cells (lower dark, higher photocurrent)	No marked effect
Deviations from stoichiometry	Sulfur deficiency	No
p doping (As)	Leads only to compensated material	Possible

the magnetic hyperfine interaction involved can hardly be used to determine σ quantitatively. However, the measurement of the perturbed angular distribution (PAD) from recoil implanted ^{54}Fe probe nuclei[14] provides a sufficiently sensitive tool to study chemical shifts in these materials.

In this paper we report on the observation of considerably negative and temperature-independent chemical shifts of iron in high-purity, synthetic pyrite and laurite single-crystal samples. The shift in pyrite corresponds to the shift observed for Fe impurities in stoichiometric RuS_2. We attribute this behavior to strong van Vleck paramagnetism as it is expected from the electronic structure calculations mentioned above. Bulk susceptibility measurements of the high-purity samples at low temperature show that the occurrence of paramagnetic moments essentially scales with magnetic impurity contamination. There is no indication for local moment formation at nonstoichiometric iron sites.

II. EXPERIMENT

The pyrite crystals were prepared by chemical vapor transport (CVT) using bromine as transporting agent. Quartz glass ampoules were filled with 3 g pyrite powder which was prepared from the elements by reacting carbonyl-iron powder (BASE, m7N) and sulfur lumps (Ventron, m6N) in a temperature gradient ΔT=870–720 K. Prior to sealing, the ampoules were evacuated to 10^{-7} mbar and filled with 15 mg bromine. They were placed into a two-shell furnace[15] where a vertical transport from the bottom to the top of the horizontally orientated ampoule occurs. The advantage of this geometry is a short transport distance and a large nucleation surface. By an endergonic transport reaction in a temperature gradient ΔT=900–850 K, crystals up to 5 mm edge length were obtained.[16] It was found that by doping of the source with arsenic at a concentration of 10^{18} cm^{-3}, the size of CVT-grown crystal could be increased to 8 mm edge length. (Arsenic is frequently present in natural pyrite.) Both arsenic- and bromine-doped crystals were employed for the PAD measurements.

Laurite crystals with surfaces up to 15 mm^2 were obtained using a high-temperature solution-growth technique (HTSG) with bismuth melt as solvent. A quartz tube was divided into a solution and a growth region by a dip and filled with RuS_2 powder which was synthesized from the elements [Ru powder (Ventron, −240 mesh, m4N7) and S lumps (Ventron, m6N)] and bismuth pieces of high-purity (m6N, Ventron) in the molar ratio 30:1. The ampoule was then evacuated to 10^{-7} mbar and sealed. The dip prevented the RuS_2 powder (ρ=6.22 g/cm^3 at 293 K) from spreading over the whole liquid Bi surface (ρ=9.33 g/cm^3 at 1273 K). The melt was allowed to homogenize at a temperature of 1272 K for 24 h. The temperature of the growth chamber was then lowered at a rate of 2 K/h to 773 K, while the temperature of the solution zone was kept at 1273 K.[17] Eventually, the laurite crystals were separated from the solvent by dissolution of bismuth in HNO_3.

Inductively coupled plasma mass spectroscopy has been used to determine the concentration of other impurity contaminations in the pyrite samples beside arsenic. Relevant impurity concentrations are obtained for the transport agent Br (300–400 ppm), for Si (100–150 ppm), for Ti (about 30 ppm), and for Mn and Co (10–30 ppm). Some of these elements may contribute to the formation of paramagnetic local moments. The concentration of other 3d element impurities such as V, Cr, Ni, Cu, and Zn was below 1 ppm. The sulfur content of the FeS_2 samples was determined by a coulometric method, and a systematic sulfur deficiency was found in natural as well as in synthetic samples.[18] The stoichiometry of the samples was FeS_{2-x} with x in the range $0.06 < x < 0.12$.

Bulk susceptibility measurements were carried out using a Faraday magnetometer in the 10 mg balance range at a magnetic field of 10 kOe. Details of the instrumentation are given in Ref. 19; part of the susceptibility data are discussed elsewhere.[18]

For the PAD measurements the samples of FeS_2 and RuS_2 were disks of 0.3 mm thickness and 2–4 mm diameter. They were mounted onto a cold tip of a continuous-flow cryostat suitable for ion implantation measurements at the heavy-ion accelerator combination VICKSI at the Hahn-Meitner-Institut.

A pulsed ^{12}C ion beam (42 MeV) directed onto a thin Sc foil (1 mg/cm^2) was used to populate the excited 10^+ isomeric state in ^{54}Fe (g_N=0.7281, $T_{1/2}$=367 ns) (Refs. 20 and 21) through the nuclear reaction ^{45}Sc(^{12}C,2np)^{54}Fe. The Fe ions are implanted deeply into the samples behind the foil by their recoil energy of about 9 MeV. The nuclear spin alignment due to the nuclear reaction leads to an anisotropic angular distribution of the γ rays in the decay of the isomeric state. The ex-

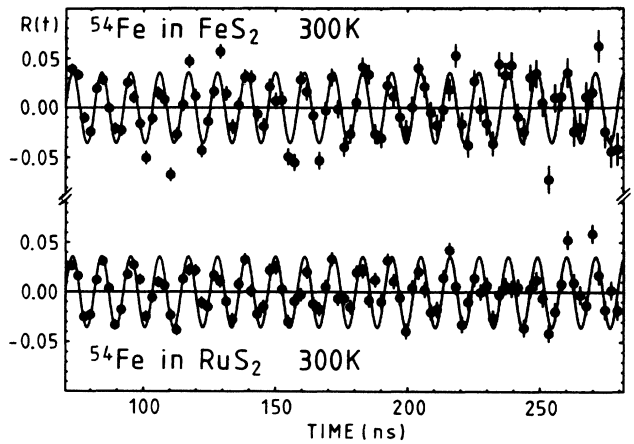

FIG. 1. Spin rotation spectra of the 10^+ isomer in ^{54}Fe implanted into FeS_2 and RuS_2 at 300 K with an externally applied magnetic field of 8.142(8) T. No damping of the spin rotation amplitude occurs within 300 ns. This time sets an upper limit for the damping rate. Two other isomers contribute to the original spin rotation pattern: the $(\frac{19}{2})^-$ isomer in ^{43}Sc ($g_N=0.3286$, $T_{1/2}=473$ ns) and the 6^+ isomer in ^{42}Ca ($g_N=-0.415$, $T_{1/2}=5.3$ ns) (Ref. 21). They are populated through nuclear reactions on sulfur isotopes in the host material itself. Fortunately, both frequencies are well separated from the frequency of the Fe nuclei. They are eliminated in this figure.

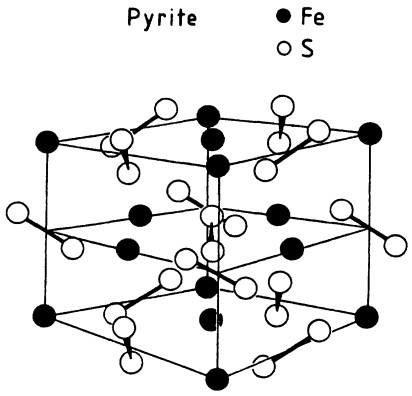

FIG. 2. Crystal structure of FeS_2 (and analogously RuS_2) (e.g., Refs. 1 and 29). The Fe ions form a fcc lattice where the electric-field gradient (efg) is zero. The neighboring S ions produce a small efg, too small to cause a measurable damping of the spin rotation amplitude within the lifetime of the isomeric ^{54}Fe state. However, if the implanted ^{54}Fe ions come to rest at nonsubstitutional sites or close to vacancies, strong efg's arise and cause a rapid decrease of the amplitude.

ponential decay is modulated in time with the Larmor precession of the nuclear spin in an externally applied magnetic field. High precision in the determination of the frequency is achieved by applying a large external field of 8.142(8) T produced by the superconducting split pair magnet SULEIMA.

From the background subtracted and normalized time spectra of the γ rays, recorded by scintillation counters, the spin rotation spectra are extracted by forming appropriate ratio functions $R(t)$.[14] Typical examples of ^{54}Fe spin rotation patterns are shown in Fig. 1. The patterns were fitted by the following expression for each frequency:

$$R(t)=\tfrac{3}{4}A_2 e^{-\lambda^2 t^2}\cos 2(\theta-\omega_L t)\ , \tag{1}$$

where ω_L is the Larmor frequency, A_2 relates to the degree of alignment retained after the implantation process, and λ is a damping parameter expressing the loss of alignment within the lifetime of the isomeric state due to radiation damage and intrinsic electric field gradients.[20] The chemical shift σ (Ref. 13) was determined according to

$$(1-\sigma)/(1-\sigma_{\rm ref})=\omega_L/\omega_{\rm ref}\ . \tag{2}$$

Here, $\omega_{\rm ref}$ is the Larmor frequency measured in a reference material, Sc metal, where the frequency shift for Fe is known with high accuracy.[22]

III. RESULTS

A well-defined Larmor frequency ω_L for Fe in the single-crystal samples of FeS_2 and RuS_2 was observed at all temperatures. The damping λ of the spin rotation amplitude was very small and we can only give an upper limit of 3×10^6 s^{-1}. However, the loss of the initial alignment was quite large. We observed a temperature-independent amplitude A_2 of only about 0.03 in pyrite as well as in laurite. This has to be compared to typical values obtained for recoil implanted Fe ions in simple metals of 0.07 (Ref. 22). The comparison of amplitudes leads to the result that about 50% of the probe nuclei experience the well-defined Larmor frequency. Since we observed almost no damping, we conclude that these and only these implanted ions substitute Fe sites in an undisturbed cubic FeS_2 environment and Ru sites in RuS_2, respectively (see Fig. 2). The other probe ions come to rest in disturbed areas, e.g., by radiation damage, and do not

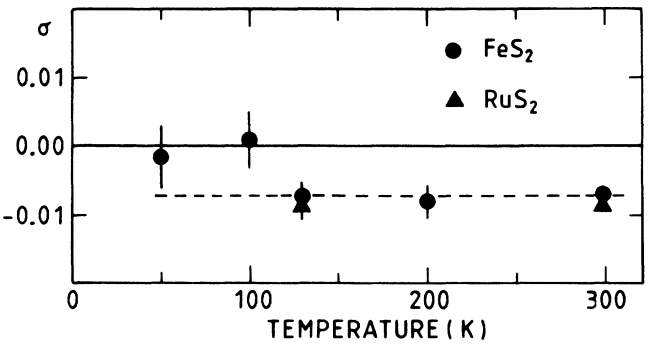

FIG. 3. Chemical shift σ at Fe nuclei in RuS_2 and FeS_2 for various temperatures. Equivalent shifts are observed in both hosts between 300 and 130 K. With the result of $\sigma=-0.008(1)$ the measured points at lower temperatures are still compatible.

TABLE II. Comparison of measured and calculated Fe chemical shifts.

Compound	σ_{expt}	σ_{theor}
FeS_2	−0.008(1)	−0.008(3)
RuS_2	−0.008(1)	

contribute to the measurement. Thus, our results are based on probe ions, which experience hyperfine interactions in *intact* crystal areas, as shall be discussed below in detail.

The chemical shifts σ obtained from the Larmor frequencies are plotted in Fig. 3 as a function of temperature. A shift of $\sigma_{expt}=-0.008(1)$ was measured at the iron nuclei in FeS_2 as well as in RuS_2. In both hosts there is no temperature dependence of σ_{expt} observed. The data are summarized in Table II.

In order to characterize our samples with conventional susceptibility measurements, we have recorded bulk susceptibility data $\chi(T)$ between 1 and 200 K for two pyrite samples. At higher temperatures, the data are quite similar to those obtained from high-purity natural samples.[4,18] A Curie-like contribution due to paramagnetic moments at low temperature was extracted according to the ansatz

$$\chi(T)-\chi_{VV}=\frac{C}{(T+\Theta)} . \tag{3}$$

We obtained best fits with $C=0.5(1)\times10^{-6}$ emuK/g, $\Theta=4(1)$ K for sample 1 and $C=0.8(1)\times10^{-6}$ emuK/g, $\Theta=6(1)$ K for sample 2. Figure 4 shows the low-temperature data. The Curie behavior is clearly seen in both samples. The amount of paramagnetic contamination may be estimated from the Curie constant C by assuming an effective magnetic moment of $5.5\mu_B$ typical for magnetic FeS.[2] The concentration of paramagnetic atoms obtained for the two samples is 16 ppm and 25 ppm, respectively, which is in the order of magnetic impurity contamination, whereas from the sulfur deficiency we would formally attribute FeS stoichiometry to a few percent of iron.[7,18]

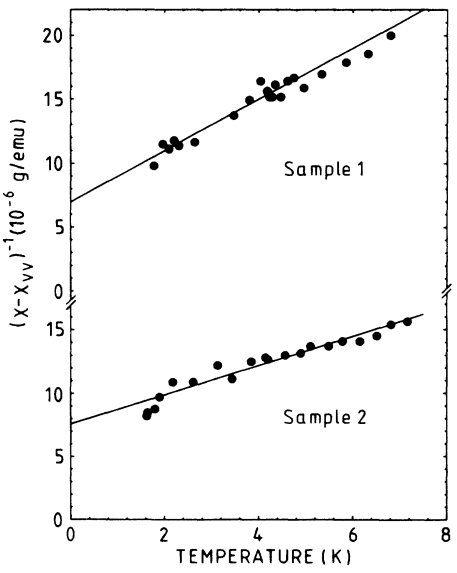

FIG. 4. Plot of the inverse susceptibility. After subtraction of the temperature independent part, $\chi(T)$ as a function of the temperature clearly reveals Curie-like behavior at low temperatures. The paramagnetic contaminations for the pyrite samples 1 and 2 are both in the ppm range. Both samples consisted of crystals grown by CVT with bromine.

IV. DISCUSSION

Before we discuss our experimental results we have to comment on the problem of radiation damage which concerns the reliability of our data. The fluence of the carbon beam is in the low dose regime ($<10^{13}$ atoms/cm^2). In addition, the beam is stopped an order of magnitude deeper (20 μm) in the sample than the Fe recoils (2 μm) for which a fluence below 10^{10} atoms/cm^2 is estimated. Therefore we are well below the borderline where amorphization and stoichiometric changes occur.[23] The recoiling ^{54}Fe ions create isolated defect cascades, and the probe ions at their final sites may be decorated in most cases with point defects, as can be deduced from the strongly reduced spin rotation amplitude.

The hyperfine interaction is very sensitive to defects in the next-nearest neighborhood. The best indication for an unperturbed final site of the ions is the observation of a well-defined Larmor frequency and above all of a damping rate consistent with the damping expected due to the intrinsic field gradients of the material. From the electric quadrupole splitting [0.62(2) mm/s] in the Mössbauer spectra of pyrite,[11] we calculate an electric-field gradient at the iron site of $V_{zz}=2.8\times10^{17}$ V/cm^2. In the spin rotation pattern we therefore expect a damping rate $\lambda=2\times10^6$ s^{-1} which agrees with the upper limit set from our data. From kinetic considerations we expect substitutional lattice sites as final resting places.[24] A considerable fraction of these implanted ions, however, may be associated with next-neighbor point defects accompanied by strong-field gradients. For this fraction, fast losses of the alignment occur. All this happens on a time scale much shorter than the lifetime of the used isomeric state and causes the amplitude of the rotation pattern to drop off. A fraction ($\approx50\%$) of the implanted Fe ions suffers such alignment losses as mentioned above.

A main advantage of local chemical shift measurements is the selective observation of the magnetic behavior of the Fe 3d electrons, whereas macroscopic measurements integrate all magnetic contributions within the compound. Paramagnetic moment formation at the iron site is ruled out by the low-temperature susceptibility data. Therefore we expect the dominance of magnetic shielding effects. The diamagnetic shift due to diamagnetic shielding of the Fe nucleus by the Fe core and 3d electrons is very small: $\sigma_{dia}=10^{-3}$–10^{-5} (Ref. 13) and can be neglected. The paramagnetic shielding (van Vleck paramagnetism) may induce shifts orders of magnitude larger: $\sigma_{VV}\sim10^{-1}$ which are quite sensitive to the electronic structure of the iron sulfur octahedron complex.

Defect states when forming a band in the gap and significantly influencing macroscopic electronic properties should also influence the paramagnetic shielding effects.

In this respect, the observation that the Fe shifts are the same in FeS_2 and in RuS_2 is a quite remarkable result. We conclude that the iron impurities form octahedral sulfur complexes with the host sulfur atoms of similar electronic structure as the iron does in pyrite. The Fe e_g state then lies in the broader Ru band gap between the Ru and Fe $2t_{2g}$ states on top of the valence band and the Ru e_g state at the bottom of the conduction band. Therefore additional optical transitions are expected to occur in Fe-doped RuS_2. Indeed, the spectral dependence of photocurrents produced with $Ru_{1-x}Fe_xS_2$ with $0<x<0.017$ was found to be dependent on the iron concentration.[25] However, photocurrent measurements on *n*-type RuS_2 (Ref. 25) show a strongly variable infrared sensitivity in the same region of wave lengths corresponding to transitions between 1.3 and 1.85 eV. The reason for this phenomenon is not clear; probably it is related to the stoichiometric variations and impurities.

In the following we estimate the shift expected from the van Vleck paramagnetism of the crystal-field split, low-spin iron state in octahedral iron sulfur complexes. The van Vleck susceptibility was calculated in an earlier work[4] on the basis of results from a linear combination of atomic orbitals (LCAO) band-structure calculation.[10] Taking the distance between the t_{2g}-band and the e_g-band midpoints to be 1.4 eV,[10] we obtain $\chi_{VV}=1\times10^{-4}$ emu/mole. The shift associated with the paramagnetic shielding is given by[26]

$$\sigma_{VV}=-2(\chi_{VV}/N_A)\xi\langle r^{-3}\rangle_{3d,\ \mathrm{atom}}\ , \tag{4}$$

where N_A is Avogadro's number, $\langle r^{-3}\rangle_{3d,\ \mathrm{atom}}$ is the expectation value of the inverse cube of the $3d$ electron radius, and ξ is a correction factor to allow for delocalization of the $3d$ electrons in the compounds. In metals, ξ is in the range between 0.5 and 1.0.[27] For the localized $3d$ orbitals in the covalent bonded FeS_2 we may take an intermediate value $\xi=\frac{3}{4}$, and with $\langle r^{-3}\rangle_{3d,\ \mathrm{atom}}=5.081$ a.u.,[28] we obtain $\sigma_{VV}=-0.008(3)$, in agreement with the experimental result. We emphasize that these estimates are uncertain with an error of about 30%. However, within this uncertainty, the selective local probe of paramagnetic shielding effects in these hosts shows results consistent with the large crystal-field split, divalent low-spin iron state. There clearly is no indication of even weak paramagnetic moments at the iron site.

Finally we comment on the problem of sulfur deficiency in pyrite. Systematic determinations of the sulfur content in natural as well as in synthetic samples have shown a sulfur deficiency in the range from 3% to 6% by atom. Formally, we deduce a ratio for FeS_2 to FeS in the range of 94:6 to 88:12. One may therefore speculate about the formation of high-spin divalent iron states, associated with defect levels in the gap. However, assuming an iron moment of $5.5\mu_B$ typical for FeS, the FeS concentration obtained from the susceptibility data would only be in the ppm region. The Curie contribution seen at low temperatures is essentially due to paramagnetic Mn and Co impurity contamination. Therefore, the formation of magnetic iron states due to sulfur deficiency is ruled out.

V. CONCLUSION

On the basis of the discussed results of a microscopic measurement, we do not see any significant qualitative difference between the local electronic structure of FeS_2 and Fe impurities in RuS_2 in the region of the forbidden energies. The chemical shifts are consistent with the crystal-field split, low-spin Fe octahedral complexes, which are known from electronic structure calculations. These results should apply as long as the materials are pure and the disulfide crystal structure is intact. However, magnetic impurities such as, e.g., Mn, Co, and Ni as well as nonmagnetic iron-defect states due to a sulfur deficiency are likely to be the source for deviations observed in bulk measurements. Therefore the task remains to investigate the influence of magnetic impurities in pyrite and to calculate the electronic structure of sulfur-deficient complexes for a more comprehensive understanding of this photovoltaic material.

ACKNOWLEDGMENTS

The authors thank Dr. U. Köbler for magnetic measurements of two pyrite samples.

[1]D. J. Vaughan and J. R. Craig, *Mineral Chemistry of Metal Sulfides* (Cambridge University Press, Cambridge, 1978), p. 96.

[2]R. C. Thiel and C. B. van den Berg, Phys. Status Solidi **29**, 837 (1968); J. L. Horwood, M. G. Townsend, and A. H. Webster, J. Solid State Chem. **17**, 35 (1976); J. R. Gosselin, M. G. Townsend, R. J. Tremblay, and A. H. Webster, *ibid.* **17**, 43 (1976).

[3]S. Miyahara and T. Teranishi, J. Appl. Phys. **39**, 896 (1968); P. A. Montano and M. S. Seehra, Solid State Commun. **20**, 897 (1976).

[4]P. Burghardt and M. S. Seehra, Solid State Commun. **22**, 153 (1977).

[5]J. D. Passaretti, K. Dwight, A. Wold, W. J. Croft, and R. R. Chianelli, Inorg. Chem. **20**, 2631 (1981).

[6]A. Ennaoui, S. Fiechter, W. Jaegermann, and H. Tributsch, J. Electrochem. Soc. **133**, 97 (1986).

[7]M.-H. Kühne and H. Tributsch, Ber. Bunsenges. Phys. Chem. **88**, 10 (1984); R. Schieck, A. Hartmann, S. Fiechter, R. Könenkamp, and H. Wetzel (unpublished); J. Luck, A. Hartmann, and S. Fiechter, Fresenius Z. Anal. Chem. **334**, 441 (1989).

[8]M. Braga, S. K. Lie, C. A. Taft, and W. A. Lester, Jr., Phys. Rev. B **38**, 10 837 (1988); S. Lauer, A. X. Trautwein, and F. E. Harris, *ibid.* **29**, 6774 (1984).

[9]W. Folkerts, G. A. Sawatzky, C. Haas, R. A. de Groot, and F. U. Hillebrecht, J. Phys. C **20**, 4135 (1987); A. Schlegel and P. Wachter, *ibid.* **9**, 3363 (1976); E. K. Li, K. H. Johnson, D. E.

Eastman, and J. L. Freeouf, Phys. Rev. Lett. **9**, 470 (1974).
[10]M. A. Khan, J. Phys. C **9**, 81 (1976).
[11]V. K. Garg, Y. S. Liu, and S. P. Puri, J. Appl. Phys. **45**, 70 (1974); E. D. Stevens, M. L. DeLucia, and P. Coppens, Inorg. Chem. **19**, 813 (1980).
[12]A. Ennaoui, S. Fiechter, H. Goslowsky, and H. Tributsch, J. Electrochem. Soc. **132**, 1579 (1985).
[13]N. F. Ramsey, Phys. Rev. **86**, 243 (1952); **78**, 699 (1950).
[14]H.-E. Mahnke, Introduction to PAC/PAD, in *Proceedings of the International Conference on Nuclear Methods in Magnetism, München, 1988,* edited by F. J. Litters and G. M. Kalvius (Baltzer, Basel, 1989), p. 77.
[15]V. Krämer, R. Nitsche, and M. Schuhmacher, J. Cryst. Growth **24/25**, 179 (1974).
[16]S. Fiechter, J. Mai, A. Ennaoui, and W. Szacki, J. Cryst. Growth **78**, 438 (1986).
[17]S. Fiechter and H.-M. Kühne, J. Cryst. Growth **83**, 517 (1987).
[18]N. Alonso Vante, G. Chatzitheodorou, S. Fiechter, N. Mgoduka, I. Poulios, and H. Tributsch, Sol. Energy Mater. **18**, 9 (1988).
[19]U. Köbler and F. Deloie, Kernforschungsanlage Jülich Report No. 1305, 1976 (unpublished).
[20]E. Dafni and G. D. Sprouse, Hyperfine Int. **4**, 777 (1978).
[21]P. Raghavan, At. Data Nucl. Data Tables **42**, 189 (1989).
[22]For calibration the temperature-independent Knight shift of $K=-\sigma_{\text{ref}}=0.020(1)$ was used. S. Seeger, H. H. Bertschat, J. Biersack, K. H. Biedermann, H. Haas, R. Kowallik, H.-E. Mahnke, W. Müller, and W.-D. Zeitz (unpublished); S. Seeger, Diplome thesis, Freie Universität Berlin, 1989 (unpublished).
[23]H. M. Naguib and R. Kelly, Radiat. Effects **25**, 1 (1975).
[24]K. D. Brice, in *Applications of Ion Beams to Materials,* IOP Conf. Ser. No. 28, edited by G. Carter *et al.* (IOP, London, 1976), p. 334.
[25]H.-M. Kühne and H. Tributsch, J. Electrochem. Soc. **130**, 1448 (1983); H.-M. Kühne, Ph.D. thesis, Freie Universität Berlin, 1985.
[26]A. M. Clogston, A. C. Gossard, V. Jaccarino, and Y. Yafet, Phys. Rev. Lett. **9**, 262 (1962).
[27]A. Abragam and B. Bleaney, *Electron Paramagnetic Resonance of Transition Ions* (Clarendon, Oxford, 1970), p. 399.
[28]A. J. Freeman and R. E. Watson, in *Magnetism,* edited by G. T. Rado and H. Suhl (Academic, New York, 1965), Vol. 2A, p. 167.
[29]J. L. Verble and R. F. Wallis, Phys. Rev. B **182**, 783 (1969).